Probing Fractal Magnetic Domains on Multiple Length Scales in $Nd_2Fe_{14}B$

A. Kreyssig,[1,2,3,*] R. Prozorov,[1,2] C. D. Dewhurst,[4] P. C. Canfield,[1,2] R. W. McCallum,[1] and A. I. Goldman[1,2]

[1]*Ames Laboratory, U.S. Department of Energy, Ames, Iowa 50011, USA*
[2]*Department of Physics and Astronomy, Iowa State University, Ames, Iowa 50011, USA*
[3]*Institut für Festkörperphysik, Technische Universität Dresden, 01062 Dresden, Germany*
[4]*Institut Laue-Langevin, 6, rue Jules Horowitz, 38042 Grenoble, France*

(Received 9 September 2008; published 29 January 2009)

Using small-angle neutron scattering, we demonstrate that the complex magnetic domain patterns at the surface of $Nd_2Fe_{14}B$, revealed by quantitative Kerr and Faraday microscopy, propagate into the bulk and exhibit structural features with dimensions down to 6 nm, the domain wall thickness. The observed fractal nature of the domain structures provides an explanation for the anomalous increase in the bulk magnetization of $Nd_2Fe_{14}B$ below the spin-reorientation transition. These measurements open up a rich playground for studies of fractal structures in highly anisotropic magnetic systems.

DOI: 10.1103/PhysRevLett.102.047204 PACS numbers: 75.60.Ch, 05.45.Df, 75.25.+z, 78.20.Ls

The industrial strength ferromagnet, $Nd_2Fe_{14}B$ has become a prototypical system for the study of magnetic domain structures. Below the Curie temperature, $T_c = 565$ K [1,2], the Nd and Fe moments order ferromagnetically. The crystal-electric field produces a strong magnetic anisotropy with the easy axis along the tetragonal **c** direction. Below the spin-reorientation temperature, $T_{SR} = 135$ K, the magnetic structure (and easy axis direction) changes via a second order transition [3] and becomes conelike [4], in which the moments are canted away from the **c** direction by an angle that increases from 0° at T_{SR} to 28° at 4 K [5,6]. The moments lie in one of the four symmetry-equivalent {1 1 0} planes in agreement with calculations of crystal-electric field effects [7]. A multitude of techniques have been used to image magnetic domains at exposed surfaces of $Nd_2Fe_{14}B$, such as Bitter decoration [8], Kerr microscopy [3,6,9–11], Lorentz [12–14] and holographic [13,15] transmission electron microscopy, scanning electron microscopy [13,16], and magnetic force microscopy [12,17–20]. For imaged surfaces perpendicular to the **c** direction, domains have been observed with dimensions between 2–5 μm at 4 K [6] and about 0.1–0.6 μm at room temperature [6,10,12], respectively. These values are very close to the single domain size of about 0.2–0.4 μm determined by magnetization measurements on polycrystalline samples [1,21].

These imaging techniques, however, only probe the magnetic fields at the surface and/or are limited in terms of the size of fine details that can be resolved. In the case of transmission electron microscopy, for example, samples thinner than 1 μm are required and the domain structure can be very different from that of a bulk specimen. Thus, important questions regarding the size, distribution and morphology of magnetic domains in the bulk remain open. Here, we address these issues by correlating the results of magnetization measurements, magnetic domain imaging, and small-angle neutron scattering experiments on solution grown $Nd_2Fe_{14}{}^{11}B$ single crystals [22,23] that manifest smooth, mirrored surfaces and can have volumes as large as 1 cm^3.

Single crystalline $Nd_2Fe_{14}{}^{11}B$ shows a strong increase in magnetization along the **c** direction below $T_{SR} = 135$ K, similar to what has been reported previously [2,5]. As shown in Fig. 1, this behavior is correlated with a dramatic change of the magnetic domain patterns above and below T_{SR} as measured by the magneto-optical Kerr effect. In both the high and the low temperature states, the domains are arranged in chains in the (**ab**) plane. However, the fine domains observed above T_{SR} evolve to much larger domains below T_{SR} [24]. Above T_{SR}, the domains exhibit more isotropic starlike boundaries whereas, below T_{SR}, the domains are nearly rectangular in shape. The Faraday microscopy patterns, shown in Fig. 2, provide a spatially resolved measurement of the local magnetization along the

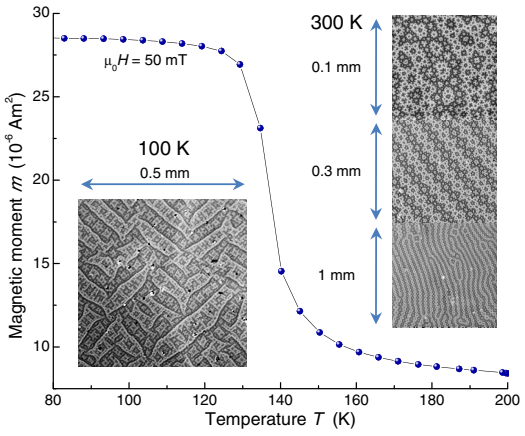

FIG. 1 (color online). Temperature dependence of the magnetization and the magnetic domain patterns in the $Nd_2Fe_{14}{}^{11}B$ single crystal. The magnetization was measured at $\mu_0 H = 50$ mT applied along the **c** axis. The magnetic domain patterns were imaged exploiting the magneto-optical polar Kerr effect at a surface perpendicular to the **c** direction and with the **a** direction vertical.

c direction. Above T_{SR}, higher values for the magnetic induction perpendicular to the surface in the inner parts of domains are observed, indicated by the red regions. This is consistent with the uniaxial alignment of moments along the **c** direction, in contrast to the canted moments below T_{SR} for which only the moment projection along the **c** direction contributes. This result appears to be in contradiction to the decreased bulk magnetization measured along the **c** direction above T_{SR}. We show below that this arises from the details of the domain structure within the bulk of the $Nd_2Fe_{14}{}^{11}B$ single crystal.

Figures 1 and 2 demonstrate clearly that domain features on many length scales can be detected at the surface of the sample. But do these features extend into the bulk? With a sufficiently large penetration depth and sensitivity to magnetic moments and magnetostrictive effects, neutrons are well suited to study this material using small-angle neutron scattering (SANS) methods. SANS measurements made with the incident neutron beam parallel to the **c** axis of the sample yield a two-dimensional Fourier transform of magnetic and magnetostrictive correlations within the (**ab**) plane of the sample, averaged over the thickness of the sample. Using well-established techniques [25], the average dimension and conformation of domains can be probed, and characteristic length scales of the magnetic induction variation can be extracted from the measurements. The minimum scattering vector of $\sim 0.5 \times 10^{-3}$ Å^{-1}, that can be realized by conventional SANS instruments, limits the dimension of detectable features to length scales smaller than ~ 1 μm, which is just at the limit of optical techniques.

SANS experiments were performed on the D11 instrument [25], at the ILL, on a platelike $Nd_2Fe_{14}{}^{11}B$ sample with its **c** direction oriented parallel to the incident neutrons. Figure 3 shows the raw SANS area-detector images both above and below T_{SR}. Even a cursory comparison of the two images reveals significant differences. First, the pattern below T_{SR} exhibits significantly more anisotropy than that above T_{SR} which is consistent with the rectangular habit of magnetic domains for $T < T_{SR}$ shown in the left panel of Fig. 1. By comparing the intensity scales in Fig. 3, it can be seen that the pattern at $T = 200$ K, above T_{SR}, exhibits significantly enhanced scattering. This indicates a strong decrease in the average domain size above T_{SR}. Perhaps most importantly, since SANS probes the distribution of magnetic domains throughout the sample, these domain distributions are characteristic of the bulk of the 300 μm thick sample, not only the exposed surface.

SANS patterns have been measured over a wide range of scattering vectors and the scattered intensity was determined as function of the magnitude of the scattering vector. The results are displayed in Fig. 4. Information regarding the formation of the magnetic domains can be obtained by fitting regions of the SANS data to a power-law behavior of the form $I = I_0 q^{\alpha}$. For details concerning the interpretation of power laws in SANS measurements, we refer the reader to several excellent reviews in Refs. [26–29]. Although we follow their treatments here, we note that much of the previous work in this area is based upon systems consisting of well defined ''objects'' with a finite homogeneous scattering strength embedded in a ''matrix'' with a different scattering strength. The situation for scattering from magnetic domains is somewhat different since the objects are the interior regions of domains with an identical and constant absolute value of the scattering strength that can be positive or negative depending on the direction of the local magnetization. The ''surfaces'' of these objects are the domain walls, with their own magnetic structure that varies across the domain wall width. Together, the domains and domain walls fill the complete volume of the sample, so no matrix in the sense used above exists.

At $T = 20$ K, the neutron scattering intensity shows a power-law dependence over a wide scattering-vector range with a single exponent α_0 from $\sim 2 \times 10^{-3}$ Å^{-1} up to $\sim 3 \times 10^{-2}$ Å^{-1}. The value of $\alpha_0 = -3.73(3)$ is not far from $\alpha = -4$ which would be the expected exponent for scattering from a ''smooth surface'', the so-called Porod scattering [26–29]. A wrinkle-free, sharp domain wall is the corresponding picture in a magnetic system. Besides

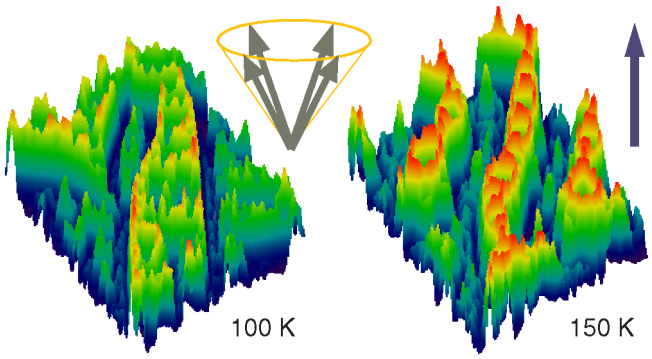

FIG. 2 (color online). Faraday images of the $Nd_2Fe_{14}{}^{11}B$ single crystal. In the transparent ferromagnetic Bi-doped Fe-garnet film placed on the surface of the sample, the distribution of the magnetic moments mimics and amplifies the magnetic induction on the sample surface. The height is proportional to the magnitude of the magnetic induction in **c** direction perpendicular to the surface. The spin structure is shown schematically.

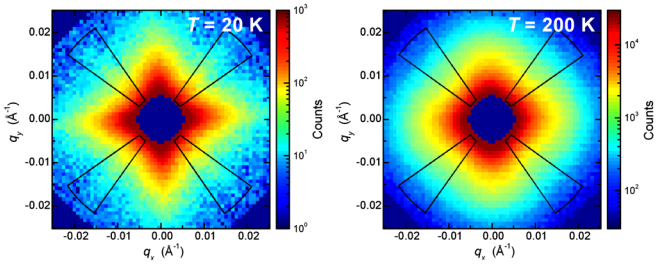

FIG. 3 (color online). Raw SANS area-detector images of the $Nd_2Fe_{14}{}^{11}B$ single crystal at temperatures of 20 K and 200 K. The colors and lines in the contour map represent the neutron counts on a logarithmic scale. The black lines mark the 20° wide sectors used for the averaging to obtain the data shown in Fig. 4.

scattering from magnetic domains, neutrons can be refracted at domain walls due to the difference in the refraction index on both sides of the domain wall. This spreading of the incident beam can cause intensity for finite scattering vectors in SANS experiments and is strongly wavelength dependent [30,31]. Contributions to the observed intensity cannot be completely excluded but measurements yield only marginal differences in the normalized intensity and deviations in α of smaller than 0.2 for scattering vectors between $\sim 2 \times 10^{-3}$ Å^{-1} and $\sim 1 \times 10^{-2}$ Å^{-1} using neutrons with wavelengths between 4 and 17 Å .

At $T = 200$ K, we see dramatic changes in the intensity and shape of the scattering curves. The number of neutrons scattered in the range between $\sim 1 \times 10^{-3}$ Å^{-1} up to $\sim 1 \times 10^{-1}$ Å^{-1} is, on average, a factor of 6 higher at $T = 200$ K than at $T = 20$ K. A distinctive kink is obvious at $\sim 1.8 \times 10^{-2}$ Å^{-1} in the curve for $T = 200$ K in contrast to the smooth shape for $T = 20$ K in the double-logarithmic plot in Fig. 4. Neutron refraction from an increased density of domain walls can yield an intensity increase but would not cause such a distinct kink. The range of scattering vectors corresponds to fine-scale features of domains from ~ 0.1 μm down to ~ 0.001 μm, well below the resolution limit of magneto-optical techniques, but close to the resolution limit of magnetic force microscopy [19,20]. These features are also significantly smaller than the domain sizes described by the branching phenomena in magnetic domains [9,11]: for a 300 μm thick $Nd_2Fe_{14}B$ single crystal, the bulk domains, at half sample thickness, are expected to be ~ 10 μm wide [9,11,32], whereas a width of ~ 0.6 μm was determined for the ''spike'' domains in near-surface regions [9,11,32]. In addition to these coarse domain structures, a complicated system of fine-scale surface domains with the topology of curved stripes with widths of 0.02–0.25 μm has also been observed by magnetic force microscopy [19,20]. Domain features on this length scale are consistent with the observed signal in the reported SANS measurement.

For a more detailed discussion of the SANS results at $T = 200$ K, it is convenient to consider two distinct q ranges denoted by the vertical lines in Fig. 4. For scattering vectors $q > q_{\mathrm{min},1} = 1.8 \times 10^{-2}$ Å^{-1}, the scattering describes the properties of the domain ''surface'' [26,27]. The observed value of $\alpha_1 = -4.84(6)$ in the power law is significantly different from $\alpha = -4$ for a sharp domain wall, with an abrupt change in the direction of the magnetization [26–29]. It falls in the class, $\alpha = -(4 + 2\beta)$ with $0 < \beta < 1$ characteristic of a ''smooth pore boundary'' [26], in which the scattering strength changes continuously over some distance by a power law with the power β. The value of $\beta = 0.42(3)$ corresponds roughly to a square-root dependence of the scattering strength in the ''boundary'' [26], close to the sinusoidal dependence expected for Bloch or Néel domain walls. The lower limit $q_{\mathrm{min},1} = 1.8 \times 10^{-2}$ Å^{-1} for this observed power-law dependence is related to the width of the domain wall [27] and yields a value of order $1/q_{\mathrm{min},1} = 6$ nm which is in excellent agreement with values of 4–9 nm determined by other methods [1,8,13,17]. The increased scattering evident at $T = 200$ K in this region, indicates that a significantly larger volume fraction of the sample is found in domain walls above T_{SR} and provides an explanation for the reduced magnetization above T_{SR} since the domain walls should not, or only marginally, contribute to the magnetization of the sample. With a strong increase in the volume fraction of domain walls in the bulk of the sample, the total magnetization measured parallel to the **c** axis is reduced above T_{SR} even though the moments are more closely aligned along the **c** axis.

In the intermediate scattering-vector range, 2.6×10^{-3} Å^{-1} $= q_{\mathrm{min},2} < q < 1.8 \times 10^{-2}$ Å^{-1} $= q_{\mathrm{max},2}$, a power $\alpha_2 = -3.09(5)$ was obtained from the SANS data measured at $T = 200$ K. The observation of a power law over a scattering-vector range of one decade with an exponent α close to -3 characterizes the scattering objects as fractals [26–29,33]. Indeed, the fractal nature may be expected for magnetic domains as we move from the two-dimensional fine surface pattern observed by Faraday imaging [34] toward the coarse three-dimensional bulk domain structures via the branching process [11]. However, the present SANS data characterize the fractal nature of magnetic domains on a submicron length scale in the bulk. Interestingly, an exponent of $\alpha \sim -3$ in the power law for the scattering data marks the boundary between two types of fractals [26–29], surface fractals with $-4 < \alpha < -3$ and volume fractals with $-3 < \alpha < -1$. A surface fractal with α close to -3 can be described as a self-affine surface, which is so strongly wrinkled, that it almost fills the three-dimensional space. The corresponding picture for a volume fractal with $\alpha \sim -3$ is that, starting from a point in a self-affine ''object'', one can find a minimum of one other point in a given maximum distance r, which is not within the same object. The range for r, over which this self-affinity can be found, corresponds to the scattering-vector range in which the specific power law is observed. Regardless of the starting point, both descriptions yield the same picture. The strong neutron scattering intensity for the intermediate scattering-vector range is related to magnetic domains in the bulk with self-affinity on a length scale from $1/q_{\mathrm{max},2} = 6$ nm to roughly $1/q_{\mathrm{min},2} = 40$ nm.

In summary, for the case of strong uniaxial anisotropy in $Nd_2Fe_{14}B$, we see that very fine magnetic domains occur at the surface and in the bulk with a self-affine geometry. Below the spin-reorientation transition, the domain structure is much coarser, less wrinkled and the effective volume of domain walls is smaller. This leads to an apparent increase of the measured magnetization along the **c** axis even though the local magnetization decreases. Small-angle neutron scattering is not only a valuable tool to characterize the conformation of magnetic domains and their domain walls, it also provides information regarding the topology of magnetic domain arrangements. Finally,

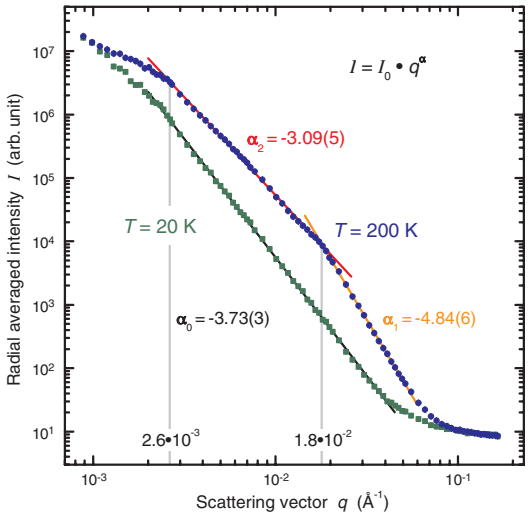

FIG. 4 (color online). Scattering-vector dependence of the SANS intensity of the $Nd_2Fe_{14}{}^{11}B$ single crystal at temperatures of 20 and 200 K. These data were determined by averaging over all four sectors marked in Fig. 3, and combining patterns measured at different sample-to-detector distances and different energies of the incident neutrons. The intensities extracted from sectors rotated by 45° to the sectors outlined in Fig. 3 are, on average, a factor of 2 larger, but show a similar dependence on the scattering vector.

we note that the magnetic properties and the corresponding magnetic domain patterns can be tuned by varying external parameters (e.g., temperature, pressure or applied magnetic field) as well as internal parameters (e.g., change of the magneto-crystalline anisotropy by substitution of different rare earths). These modifications can be isotropic or anisotropic providing a rich and almost unique opportunity for experimental studies of (magnetic) fractals.

The authors are indebted to Y. Janssen and S. Nandi for stimulating discussions. Work at the Ames Laboratory was supported by the Department of Energy, Basic Energy Sciences, under Contract No. DE AC02-07CH11358. A. Kreyssig acknowledges the support by Deutsche Forschungsgemeinschaft through SFB 463. R. Prozorov acknowledges support by the NSF Grant No. DMR 05-53285 and by the Alfred P. Sloan foundation.

*kreyssig@ameslab.gov

[1] K. H. J. Buschow, Mater. Sci. Rep. **1**, 1 (1986).
[2] J. F. Herbst, Rev. Mod. Phys. **63**, 819 (1991).
[3] Y. G. Pastushenkov, Z. Metallkd. **93**, 991 (2002).
[4] N. Inaba, H. Miyajima, and S. Chikazumi, Jpn. J. Appl. Phys. **27**, 947 (1988).
[5] K. Tokuhara, Y. Ohtsu, F. Ono, O. Yamada, M. Sagawa, and Y. Matsuura, Solid State Commun. **56**, 333 (1985).
[6] Y. G. Pastushenkov, A. Forkl, and H. Kronmüller, J. Magn. Magn. Mater. **174**, 278 (1997).
[7] M. Yamada, H. Kato, H. Yamamoto, and Y. Nakagawa, Phys. Rev. B **38**, 620 (1988).
[8] W. D. Corner and M. J. Hawton, J. Magn. Magn. Mater. **72**, 59 (1988).
[9] R. Szymczak, D. Givord, and H. S. Li, Acta Phys. Pol. A **72**, 113 (1987).
[10] L. Folks, R. Street, and R. C. Woodward, Appl. Phys. Lett. **65**, 910 (1994).
[11] A. Hubert and R. Schäfer, *Magnetic Domains. The Analysis of Magnetic Microstructures* (Springer-Verlag, Berlin, Germany, 2000), Chap. 3.7.5 and Chap. 5.2.1.
[12] H. Lemke, T. Göddenhenrich, C. Heiden, and G. Thomas, IEEE Trans. Magn. **33**, 3865 (1997).
[13] Y. Zhu and M. R. McCartney, J. Appl. Phys. **84**, 3267 (1998).
[14] Y. Shinba, T. J. Konno, K. Ishikawa, K. Hiraga, and M. Sagawa, J. Appl. Phys. **97**, 053504 (2005).
[15] Y.-G. Park and D. Shindo, J. Electron Microsc. **53**, 43 (2004).
[16] J.-Y. Wang, L. H. Lewis, D. O. Welch, and P. Canfield, Mater. Charact. **41**, 201 (1998).
[17] P. Grütter, E. Meyer, H. Heinzelmann, L. Rosenthaler, H.-R. Hidber, and H.-J. Güntherodt, J. Vac. Sci. Technol. A **6**, 279 (1988).
[18] V. Neu, S. Melcher, U. Hannemann, S. Fähler, and L. Schultz, Phys. Rev. B **70**, 144418 (2004).
[19] W. Szmaja, J. Magn. Magn. Mater. **301**, 546 (2006).
[20] M. Al-Khafaji, W. M. Rainforth, M. R. J. Gibbs, J. E. L. Bishop, and H. A. Davies, J. Appl. Phys. **83**, 6411 (1998).
[21] M. Grönefeld and H. Kronmüller, J. Magn. Magn. Mater. **88**, L267 (1990).
[22] P. C. Canfield and Z. Fisk, Philos. Mag. B **65**, 1117 (1992).
[23] P. C. Canfield and I. R. Fisher, J. Cryst. Growth **225**, 155 (2001).
[24] See EPAPS Document No. E-PRLTAO-102-001907 for real-time videos with Faraday and Kerr images of magnetic domains in $Nd_2Fe_{14}B$ as function of temperature. For more information on EPAPS, see http://www.aip.org/pubservs/epaps.html.
[25] P. Lindner, R. P. May, and P. A. Timmins, Physica (Amsterdam) **180–181B**, 967 (1992).
[26] P. W. Schmidt, in *The Modern Aspects of Small-Angle Scattering*, edited by H. Brumberger (Kluwer Academic, Dordrecht, Netherlands, 1995), p. 1.
[27] D. F. R. Mildner and P. L. Hall, J. Phys. D **19**, 1535 (1986).
[28] P. W. Schmidt, in *The Fractal Approach to Heterogeneous Chemistry*, edited by D. Avnir (John Wiley and Sons, Chichester, UK, 1989), Chap. 2.2.
[29] J. E. Martin and A. J. Hurd, J. Appl. Crystallogr. **20**, 61 (1987).
[30] O. Schärpf, J. Appl. Crystallogr. **11**, 626 (1978), and references therein.
[31] A. Hoffmann and G. P. Felcher, in *Handbook of Magnetism and Advanced Magnetic Materials*, edited by H. Kronmüller and S. Parkin (John Wiley & Sons, Hoboken, NJ, USA, 2007), Vol. 3.
[32] H. Kronmüller and M. Fähnle, *Micromagnetism and the Microstructure of Ferromagnetic Solids* (Cambridge University Press, Cambridge, England, 2003), Chap. 9.2.6.
[33] A fractal object remains similar to itself after an isotropic change of scale or dilation. For "self-affine" objects, this dilation can be anisotropic with different scaling factors for different directions [27].
[34] B.-S. Han, D. Li, D.-J. Zheng, and Y. Zhou, Phys. Rev. B **66**, 014433 (2002).